water

MDPI

Article

Photocatalytic Removal of the Antibiotic Furazolidone Using g-C_3N_4 in the Presence of Persulfates Under Lab and Pilot Scale Conditions

Christina Efthymiou [1], Christos Lykos [1], Vasiliki Boti [1,2,*], Ioannis Konstantinou [1,2,*] and Triantafyllos Albanis [1,2]

[1] Department of Chemistry, University of Ioannina, 45110 Ioannina, Greece; ch.evthymiou@uoi.gr (C.E.); c.lykos93@gmail.com (C.L.); talbanis@uoi.gr (T.A.)

[2] Unit of Environmental, Organic and Biochemical High-Resolution Analysis–Orbitrap-LC–MS, University of Ioannina, 45110 Ioannina, Greece

* Correspondence: vboti@uoi.gr (V.B.); iokonst@uoi.gr (I.K.)

Abstract: Furazolidone, a nitrofuran antibiotic, has been broadly used in aquaculture and veterinary medicine, and its presence in water poses considerable environmental and health hazards due to its toxicity. This study investigated a hybrid photocatalytic process for the removal of furazolidone, employing graphitic carbon nitride (g-C_3N_4) and persulfate anions (PS) under both laboratory and pilot-scale conditions. The synergistic effect of g-C_3N_4 and PS enhanced the generation of reactive species, facilitating the efficient degradation of FZ in two different aqueous matrices. Through scavenging studies, positive holes were determined to be the dominant reactive species, followed by sulfate radicals. Seven transformation products of FZ were tentatively identified via UHPLC-LTQ/Orbitrap MS analysis. The optimized photocatalytic system (g-C_3N_4/PS) achieved a 100% removal of furazolidone in less than 60 min under simulated solar light, demonstrating its potential for large-scale application in wastewater remediation. Furthermore, pilot-scale experiments using real secondary treated municipal wastewater proved that the applied process is capable of achieving an 86.2% removal of furazolidone ($k = 0.017$ min^{-1}) as well as a 90% decrease in effluent ecotoxicity within 120 min of UV_A irradiation. This study provides insights into sustainable processes for the removal of antibiotic contaminants from wastewater and underscores the role of g-C_3N_4-based photocatalytic approaches in upper-scale applications.

Keywords: photocatalysis; g-C_3N_4; persulfate; furazolidone; transformation products; toxicity assessment; pilot-scale

Academic Editor: Gongduan Fan

Received: 9 January 2025
Revised: 11 February 2025
Accepted: 18 February 2025
Published: 19 February 2025

Citation: Efthymiou, C.; Lykos, C.; Boti, V.; Konstantinou, I.; Albanis, T. Photocatalytic Removal of the Antibiotic Furazolidone Using g-C_3N_4 in the Presence of Persulfates Under Lab and Pilot Scale Conditions. *Water* **2025**, *17*, 602. https://doi.org/10.3390/w17040602

1. Introduction

Natural water resources are under escalating pressure owing to ever-increasing human activity (e.g., urbanization, industry, agriculture, and animal husbandry), which has detrimental effects on the health of aquatic ecosystems [1–4]. According to various reports, emerging contaminants (ECs) from human activities, like pharmaceuticals, pesticides, industrial chemicals, and other organic micropollutants, contribute significantly to the contamination of natural water bodies, negatively affecting aquatic life [5,6]. The introduction of ECs into environmental aqueous matrices is mainly attributed to conventional wastewater treatment plant (WWTP) effluents and their failure to remove such compounds at satisfactory levels [7,8]. Therefore, the development and implementation of non-conventional wastewater processing techniques in WWTPs have been extensively studied as an alternative pre- or post-treatment stage that has the potential to adequately remove/transform ECs and improve the overall effluent quality [9–11].

Heterogeneous photocatalysis is a widely used and applied advanced oxidation process (AOP) for the non-selective degradation of organic pollutants. This process generates in situ reactive species ($HO^{\bullet}$, $O_2^{\bullet-}$, $^1O_2$, etc.) utilizing semiconductors (i.e., photocatalysts) in the presence of solar light and water [12,13]. In recent years, visible-light-activated (VLA) photocatalysts have attracted significant interest in the field of photocatalysis as compared to the traditional titanium dioxide (TiO_2), which can only be photoactivated under UV radiation (~3–5% of the solar spectrum), they can harness more solar light due to their narrower band-gaps (E_g) [14–16]. Graphitic carbon nitride (g-C_3N_4) is a novel, polymeric, two-dimensional (2D) semiconducting material that can be easily synthesized via pyrolysis of common organic compounds abundant in nitrogen (urea, melamine, thiourea, etc.). It demonstrates a range of appealing characteristics such as non-toxicity, high thermal and chemical stability, and a relatively narrow E_g (~2.7 eV) that enables its photoactivation under visible light, making it ideal for environmental photocatalytic applications under solar light [17–21].

In addition to heterogeneous photocatalysis, AOPs based on sulfate radical generation (SR-AOPs) are of increasing interest for applications in WWTPs due to the exceptional reactivity of sulfate radicals ($SO_4^{\bullet-}$) (E° = 2.6–3.1 V) towards numerous organic compounds, as well as their greater stability over a broad pH range and a long half-life time compared to $HO^{\bullet}$ [22,23]. The predominant methodologies for the formation of $SO_4^{\bullet-}$ include the dissolution of salts containing persulfate (PS) or peroxymonosulfate (PMS) anions in aqueous matrices and the application of energy-intensive techniques such as sonication or heating to induce homolytic cleavage of the peroxide bond [24–26]. Another traditional method to produce $SO_4^{\bullet-}$ using either PS or PMS employs dissolved transition metal cations (e.g., Fe^{2+}, Ni^{2+}, and Co^{2+}), which cause the cleavage of the peroxide bond through electron transfer in a homogeneous catalytic system [27–29]. Although both the above-mentioned approaches are effective in activating PS and PMS anions, their utilization in larger-scale applications is questionable from an environmental point of view, as in the former case, a large amount of energy is required, while in the latter case, the presence of residual transition metal cations in wastewater after processing can lead to secondary pollution [23,27,30]. An alternative method for PS activation that can overcome these limitations is photocatalysis, as the photogenerated electrons can be transferred to the PS anions adsorbed on the surface of the photocatalysts, thereby causing the cleavage of the peroxide bond [31,32]. Additionally, solar light (UV photons) can cause the homolytic breakdown of this bond, further increasing the formation rate of $SO_4^{\bullet-}$ [23,29,33]. A number of studies have proven that the hybridization of photocatalysis with PS exhibits exceptional performance in the removal of ECs from aqueous matrices [27,34,35].

Furazolidone (FZ) is an antibiotic belonging to the nitrofuran (NF) group that has been used globally against protozoan and Helicobacter pylori infections, in both medicine and livestock [36]. This compound is rapidly metabolized in animals, resulting in the formation of its main metabolite, 3-amino-2-oxazolidinone (AOZ), within a few hours, which is linked to tissue proteins and persists with a long half-life [37]. Both the parent compound and its metabolites exhibit carcinogenic and mutagenic activities; hence, they are presently prohibited in food-producing animals [38,39]. Nonetheless, it continues to be applied because of its significant efficacy and low cost, and studies are being conducted to further explore its therapeutic actions [40–44].

To date, there is limited data concerning the degradation of FZ in aquatic systems [45–49], while there are no available studies on the photocatalytic removal of FZ from the perspective of an upper-scale application, compared to other antibiotics [50–56]. Pilot-scale studies are essential for demonstrating the practical relevance of photocatalytic methods for the elimination of antibiotics from complex aqueous matrices. In particular, Lykos et al. demonstrated the effective degradation of metronidazole utilizing a CPC pilot plant in the presence of g-C_3N_4, achieving over a 91% elimination while also decreasing ecotoxicity [50]. Similarly, Fotiou et al. emphasized the elimination of fluoxetine from hospital wastewater, demonstrating the efficacy of TiO_2 photocatalysis in reducing bioconcentration and toxicity under practical conditions [57]. Moles et al. underscored the scalability of TiO_2/UV-Vis systems by attaining up to a 100% elimination of antibiotics, including azithromycin and amoxicillin, from wastewater treatment plant effluents, while also exhibiting efficient catalyst recovery [55]. Almansba et al. presented an innovative bright textile photoreactor that markedly improved the degradation efficiency and compactness, demonstrating practical application at a pilot scale [58], while Cabrera-Reina et al. investigated the degradation of imipenem and meropenem utilizing natural solar radiation and a CPC reactor, validating the viability of the process for actual aqueous matrices and its effectiveness in minimizing energy demands [56]. These studies emphasize the significance of pilot-scale research in joining laboratory experiments with potential, upper-scale environmental applications, thereby ensuring the scalability and sustainability of photocatalytic processes.

In this light, the present work focused on the photocatalytic removal of the antibiotic furazolidone using urea-derived g-C_3N_4, in the presence or absence of PS anions. Initially, lab-scale experiments were carried out using either ultrapure water (UPW) or secondary treated municipal wastewater (SWW) as a matrix, spiked with a relatively high concentration of FZ to compare the efficiency of the applied processes and facilitate the detection and identification of FZ's transformation products (TPs) using UHPLC–LTQ/Orbitrap MS/MS. Next, pilot-scale experiments were conducted using both g-C_3N_4 and PS under UV_A radiation for the degradation of an environmentally relevant concentration of FZ, to evaluate the scalability of the process for real-world applications. The hybrid technique exhibited enhanced removal efficiency of the model pollutant in all cases (laboratory- and pilot-scale). In addition, two in-silico tools and an in vitro toxicity assessment methodology were applied to assess the detoxification effect of the hybrid g-C_3N_4/PS photocatalytic approach and to better understand the impact of the applied method on effluent quality. To the extent of our knowledge, this is the first pilot-scale study utilizing g-C_3N_4 and PS simultaneously for the hybrid photocatalytic treatment of SWW.

2. Materials and Methods

2.1. Reagents and Material

Material and reagents are described in detail in Supplementary Material (S1). The synthesis protocol and characterization of urea-derived g-C_3N_4 have been detailed in our previous publication [59]. The main physicochemical properties of g-C_3N_4 were as follows: S_{BET} = 82.3 m^2 g^{-1}, mean hydrodynamic diameter = 314 nm, Eg = 2.83 eV.

2.2. Photolytic and Photocatalytic Experiments

Lab-scale photolytic and photocatalytic experiments were conducted utilizing a Suntest CPS+ apparatus supplied by Atlas (Linsengericht, Germany), which was equipped with a 1500 W xenon arc lamp covered with a UV cut-off filter blocking wavelengths below 290 nm. The physicochemical characteristics of the SWW sample used for the lab and pilot-scale study are described in Table S1. A 100 mL solution of FZ (10 mg L^{-1}) was prepared in either UPW or SWW, transferred to a double-walled glass photoreactor installed in the center of the irradiation chamber, and magnetically stirred throughout the study. Furthermore, a concentration of 100 mg L^{-1} g-C_3N_4 was introduced into the photoreactor, whereas in the PS photoactivation experiments, ~24 mg (1 mM) of PS was dissolved in the FZ solution. Also, when g-C_3N_4 was used, the mixture was stirred in the dark for half an hour before being illuminated to reach the adsorption–desorption equilibrium of FZ on the photocatalyst surface. In the case of the hybrid experiments (g-C_3N_4/PS), the above-mentioned amount of g-C_3N_4 was added to the photoreactor and after 30 min of stirring in the dark, approximately 24 mg of PS was dissolved in the suspension, and illumination was initiated. The simulated solar radiation intensity (I) was maintained at 500 W m^{-2} for 60 min of irradiation. At designated time intervals, 5 mL aliquots of the reactor contents were collected, filtered through a 0.22 μm PTFE syringe filter, and stored in 7 mL glass vials at 4 °C until further analysis. Additionally, 25 μL of MeOH was added to each sample when PS was used as an oxidant to quench the reaction. All photolytic and photocatalytic experiments were performed in triplicate to evaluate the reproducibility of the applied processes.

Pilot-scale tests were conducted using an Ecosystem ACADUS (Mod. 10/85) in-lab pilot photoreactor (LPP) (Barcelona, Spain), as detailed in our previous study [57]. First, 60 L of SWW was transferred to the recirculation tank, spiked with FZ (250 μg L^{-1}), and stirred for 15 min. Subsequently, 6 g (100 mg L^{-1}) of g-C_3N_4 and/or 14.3 g (1 mM) of PS were introduced into the tank and stirred for another 15 min in the absence of light. The pump was then activated, and the suspension was recirculated into the irradiation chamber for 30 min before exposure to UV_A radiation. In total, the irradiation process lasted 120 min, during which samples (200 mL) of the reactor contents were collected at fixed time intervals. The samples were vacuum filtered using 0.45 μm nylon filters and stored at a low temperature (approximately 4 °C) until extraction on the same day.

2.3. Analytical Procedures

2.3.1. Sample Preconcentration Protocol with SPE

Before high-resolution mass spectrometric analysis, the samples acquired during the photolytic and photocatalytic experiments (lab- and pilot-scale) were preconcentrated by SPE, to facilitate the identification of TPs. First, Oasis HLB cartridges (200 mg, 6 cm^3) were installed on top of the extraction manifold and conditioned with 5 mL of MeOH and 5 mL of H_2O. Samples (5 mL for lab or 40 mL for pilot) were then loaded into the cartridges at a flow rate of 1 mL min^{-1}. The cartridges were then left to dry for 20 min under a vacuum, after which the analytes were eluted with 2 × 5 mL of MeOH. The eluents were condensed to dryness under a mild nitrogen flow and reconstituted in 250 μL H_2O: MeOH (80:20 *v*/*v*).

2.3.2. Determination of Residual FZ Concentration Using High-Performance Liquid Chromatography (HPLC)

The concentration of FZ during photolytic and photocatalytic experiments was studied using an HPLC system provided by Shimadzu (Kyoto, Japan), which consisted of a solvent delivery pump (LC-10AD), a degasser unit (DGU-14A), an auto-sampler (SIL-20A), a photodiode array detector (SPD-M10A), and a column oven (CTO-10A), interfaced with a PC via the communication bus module (CBM-20A). The chromatographic analysis was accomplished using a Supelco Discovery C18 column (15 mm × 4.6 mm, 5 μm particle size) (Bellefonte, PA, USA). The mobile phase consisted of a mixture of (A) water (HPLC) + 0.1% FA and (B) acetonitrile + 0.1% FA (A:B = 65:35%, isocratic elution) operating at a constant flow rate and column temperature of 1 mL min^{-1} and 40 °C, respectively. UV detection of FZ was performed at 360 nm (limit of quantification of FZ ≅ 0.1 mg L^{-1} for undiluted samples).

2.3.3. Detection and Identification of FZ's TPs Using UHPLC—LTQ/Orbitrap Mass Spectrometry

A Thermo Fisher Scientific Accela UHPLC system (Bremen, Germany) coupled with a hybrid LTQ-FT Orbitrap XL 2.5.5 SP1 mass spectrometer with an electrospray ionization (ESI) source was used for the detection and tentative identification of TPs formed during hybrid g-C_3N_4/PS photocatalytic removal of FZ. The separation of FZ and its TPs was carried out using a Thermo Fisher Scientific Hypersil Gold C18 analytical column (100 × 2.1 mm, 1.9 μm particle size) (Bremen, Germany). The gradient program used water + 0.1% FA (A) and methanol + 0.1% FA (B) as the mobile phases (Table S2). Column temperature, flow rate, and injection volume were set at 35 °C, 0.4 mL min^{-1}, and 10 μL, respectively. In positive ionization mode (PI), the compounds were identified in the mass range of 100–1000 Da with a mass resolving power of 60,000 FWHM. The ESI-MS parameters are listed in detail in Supplementary Material, Table S3.

2.3.4. In Vitro Monitoring of Ecotoxicity Using the Microtox Bioassay

In vitro ecotoxicological assessment of the samples obtained during the hybrid photocatalytic process was performed using the Microtox bioassay utilizing the marine bacterium *Vibrio fischeri* (*V. fischeri*) and an Azur Environmental m500 Analyzer (Carlsbad, CA, USA). MicrotoxOmni v1.18 software was used to evaluate samples' ecotoxicity (bioluminescence inhibition) according to the 81.9% Basic Test protocol.

Toxicity assessments using this protocol rely on the bioluminescent property of *V. fischeri*, which is driven by the enzyme luciferase during metabolic activity. Exposure to a toxic environment disrupts metabolic processes, reducing bioluminescence intensity. After 15 min of incubation, the degree of bioluminescence reduction reflects the sample's ecotoxicity, with greater reductions corresponding to higher bioluminescence inhibition [60].

2.3.5. In Silico Ecotoxicological Risk Assessment for FZ and Its TPs

The ecotoxicity of FZ and its tentatively identified TPs at three different aquatic trophic levels was assessed in silico using the Ecological Structure–Activity Relationship Model (ECOSAR v2.0) developed by the U.S. Environmental Protection Agency (EPA). Specifically, the software predicts the acute (LC_{50} or EC_{50}) and chronic (ChV) toxicity values of organic compounds in fish, daphnids, and green algae using quantitative structure–activity relationship (QSAR) models. The Globally Harmonized System of Classification and Labeling of Chemicals was used to classify each compound as either very toxic (ChV, LC_{50} or EC_{50} $\leq$ 1 mg L^{-1}), toxic (1 mg L^{-1} < ChV, LC_{50} or EC_{50} $\leq$ 10 mg L^{-1}), harmful (10 mg L^{-1} < ChV, LC_{50} or EC_{50} $\leq$ 100 mg L^{-1}), or not harmful (ChV, LC_{50} or EC_{50} $\geq$ 100 mg L^{-1}) to the corresponding trophic level.

Similarly to ECOSAR v2.0, the Toxicity Estimation Software Tool v5.1.2 (T.E.S.T.) (also developed by U.S. E.P.A.) was used for the in silico estimation of mutagenicity and developmental toxicity values for FZ and its TPs using QSAR models. It should be noted that the consensus method was chosen because it is expected to generate the most accurate results, according to the manufacturer. Additionally, predicted values above 0.50 were considered positive for either mutagenicity or developmental toxicity.

3. Results

3.1. Photocatalytic Degradation of FZ with g-C_3N_4 in the Presence of PS (Lab and Pilot-Scale)

The degradation rate of FZ using either g-C_3N_4 or PS separately, as well as in combination (g-C_3N_4/PS), was first studied under lab-scale conditions using UPW or SWW as an aqueous matrix to compare the performance of each process. To assess the impact of simulated solar light on the photolytic degradation of FZ, experiments were conducted without g-C_3N_4 and PS using the same lab-scale methodology. The removal kinetics, shown in Figure 1a,b, were modeled using a pseudo-first-order kinetic approach ($R^2 > 0.97$), with the corresponding kinetic data summarized in Table S4. It should be noted that the percent relative standard deviation (%RSD) was lower than 7% in all lab-scale experiments, suggesting that good reproducibility of the results was achieved (n = 3).

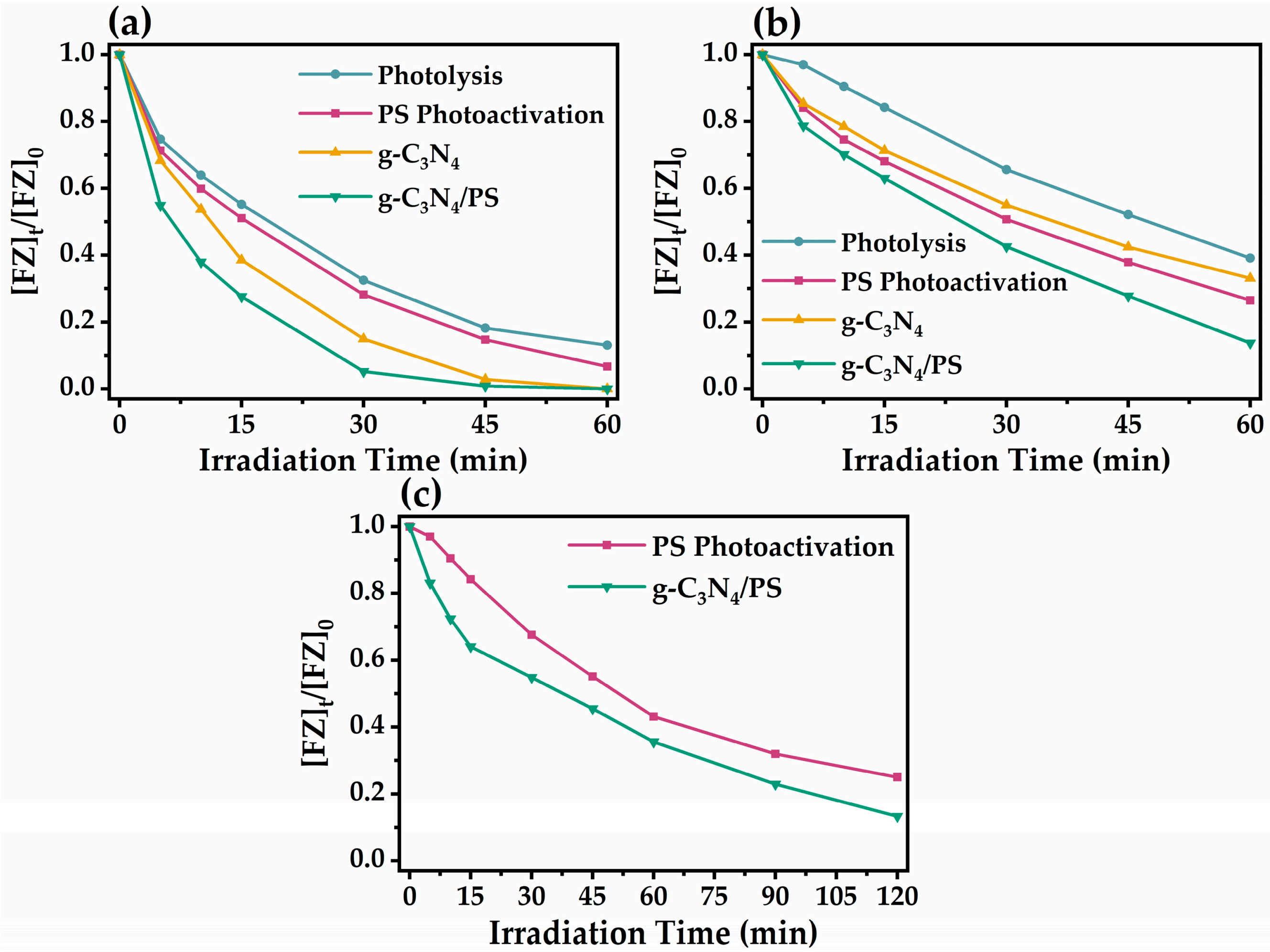

Figure 1. Removal of FZ (10 mg L^{-1}) under simulated solar radiation (I = 500 W m^{-2}) in the presence or absence of g-C_3N_4 (100 mg L^{-1}), PS (1 mM), or g-C_3N_4/PS using (**a**) UPW or (**b**) SWW as an aqueous matrix. (**c**) Pilot-scale removal of FZ (250 µg L^{-1}) from SWW using PS (1 mM) or g-C_3N_4/PS (10 mg L^{-1}/1 mM) under UV_A radiation.

All processes showed increased efficiency in terms of FZ removal compared to photolysis alone in both UPW and SWW. As expected, using SWW as the aqueous matrix significantly reduced the degradation rate of FZ in all processes compared to UPW, due to the various components of SWW, such as dissolved organic matter (DOM) and dissolved anions acting as scavengers for the reactive species generated [61–63]. Additionally, suspended solids (SS) and DOM in SWW can act as light filters, limiting light penetration into the aqueous matrix and thus reducing the efficiency of different photo-processes [64,65]. The simultaneous use of g-C_3N_4 and PS (hybrid) demonstrated the greatest efficiency among all the processes tested, achieving the complete removal of the antibiotic in UPW and a satisfactory 86.7% removal rate in SWW. According to the kinetic data summarized in Table S4, the applied hybrid photocatalytic process was 2.4 and 1.3 times faster than PS photoactivation when UPW and SWW were used as matrices, respectively. Moreover, compared to g-C_3N_4 photocatalysis, the g-C_3N_4/PS hybrid approach achieved 1.4 times faster kinetics in both matrices. These findings align with similar studies that employed g-C_3N_4 and PS for the removal of various organic pollutants, including dyes and antibiotics. In all cases, the synergistic effect between g-C_3N_4 and PS led to significantly improved removal rates compared to the stand-alone processes [66–70]. It appears that the use of oxidants, such as PS, in combination with photocatalysts (e.g., g-C_3N_4) is also a viable approach to partially limit the recombination rate of photogenerated holes (h^+) and electrons owing to the rapid reaction between oxidant and electrons on the photocatalyst surface, further improving the efficiency of the system [70,71].

Interestingly, photocatalysis with g-C_3N_4 exhibited the second-highest performance in UPW, followed by PS photoactivation, whereas the opposite was observed for SWW. This effect is likely due to DOM adhering to the g-C_3N_4 surface when SWW is used, which obstructs the mass transfer of FZ to the photocatalyst and restricts its interaction with reactive species. Considering that PS photoactivation is a homogeneous process, such limitations have not been applied.

The effect of oxidant concentration on the degradation efficiency of the hybrid method was investigated by conducting lab-scale experiments using different concentrations of PS (1, 0.75, and 0.5 mM). It should be noted that higher concentrations of PS were not investigated, as they could potentially lead to elevated sulfate concentration of the matrix in levels that can cause environmental problems such as increased conductivity, potential for corrosion and in general perturbation in the balance of the natural sulfur cycle [72]. The kinetic results (Table S5) showed a slight decrease in the removal kinetics of FZ for 0.75 (−6.4%) and 0.5 mM (−9.7%), compared to the initial PS concentration (1 mM). Therefore, these data indicate that 1 mM is the optimum concentration of PS when a relatively low concentration of g-C_3N_4 is used. However, since satisfactory FZ removal was also achieved with lower amounts of oxidant, it could be concluded that in a large-scale application, a smaller dose of PS could be chosen combined with g-C_3N_4 to limit operational costs.

To elucidate which reactive species dominated the photocatalytic degradation of FZ when the hybrid approach was applied, scavenging experiments were conducted using MeOH ($k_{SO4\bullet-} = 7.7 \times 10^7\ M^{-1}s^{-1}$, $k_{HO\bullet} = 1.2 \times 10^9\ M^{-1}s^{-1}$), oxalate anions ($C_2O_4^{2-}$) (for h^+), and L-histidine ($k_{HO\bullet} = 5.0 \times 10^9\ M^{-1}s^{-1}$, $k_{1O2} = 3.2 \times 10^7\ M^{-1}s^{-1}$) [71,73,74]. The corresponding kinetic data are presented in Table 1, which indicate that h^+ was the predominant reactive species as the addition of $C_2O_4^{2-}$ resulted in a 20.4% inhibition of FZ removal kinetics. Interestingly, the presence of L-histidine had a negligible effect on the removal of FZ, suggesting that both $HO^\bullet$ and $^1O_2$ contributed less to the degradation mechanism than h^+. Finally, the addition of MeOH resulted in a 9.7% decrease in the degradation rate of FZ, which was attributed to the quenching of $SO_4^{\bullet-}$ because $HO^\bullet$, as mentioned above, did not play a key role in the removal of the antibiotic. In conclusion, the experiments indicated that FZ was mainly degraded by h^+ and secondarily by $SO_4^{\bullet-}$. This was further substantiated by comparing the kinetic results of individual processes. In particular, the photocatalytic removal of FZ with g-C_3N_4, in which h^+ plays a key role, was 1.7 times faster than the removal observed during the photoactivation of PS, where $SO_4^{\bullet-}$ is mainly generated.

Table 1. Removal kinetic constants (k), half-life values ($t_{1/2}$), correlation coefficients (R^2), and percentage inhibition of FZ removal rate per scavenger.

Scavenger	k (min^{-1})	R^2	$t_{1/2}$ (min)	Inhibition (%)
None	0.103	0.9914	6.7	-
MeOH	0.093	0.9928	7.5	9.7%
$C_2O_4^{2-}$	0.082	0.9927	8.5	20.4%
L-histidine	0.101	0.9934	6.9	1.9%

The influence of common wastewater constituents on FZ removal kinetics was assessed by systematically investigating the effect of nitrate (NO_3^-), chloride (Cl^-), and sulfate (SO_4^{2-}) anions in the presence of PS (1 mM) and g-C_3N_4 (100 mg L^{-1}) using UPW as the matrix in lab-scale experiments. It should be noted that the concentrations of anions studied in this case were chosen according to their concentrations detected in the SWW sample (Table S1). The results (Table S6) indicated that Cl^- and SO_4^{2-} exhibit an inhibitory effect on FZ degradation, possibly due to their ability to quench radicals [23] as well as scavenge h^+ [59], thereby altering the system efficiency. In particular, Cl^- tends to react with $SO_4^{\bullet-}$ and $HO^{\bullet}$, generating chlorine radicals ($Cl^{\bullet}$) [72], which have a lower oxidation potential and can also attack Cl^- or combine to form molecular chlorine (Cl_2) [75], thereby limiting the available reactive species in the system. Interestingly, in the case of NO_3^-, a slight increase in FZ removal kinetics was observed. This could be attributed to $HO^{\bullet}$ generation from NO_3^- in the presence of hydrogen cations (H^+) under the effect UV light irradiation [76,77], which could then rapidly react with FZ, increasing the removal rate. Although NO_3^- are expected to scavenge reactive species such as h^+ [75], it appears that the above-mentioned phenomenon is more dominant. Overall, the kinetic analysis revealed variations in reaction rates depending on the anion type, highlighting the complex interplay between inorganic ions and photocatalytic processes in real water matrices.

In most studies focusing on the application of AOPs (heterogeneous photocatalysis, oxidant activation, photo-Fenton, etc.) for wastewater remediation, lab-scale experiments are carried out as proof-of-concept approaches to evaluate the performance of the applied process (removal kinetics, formation of TPs, TOC removal, ion formation, etc.), using unrealistically high concentrations of target pollutants (dyes, pharmaceuticals, pesticides, etc.) and low volumes of spiked wastewater (e.g., 50–500 mL). Although this is understandable, especially in studies focusing on the detection and identification of TPs, from a practical point of view, this could lead to many misinterpretations, as various parameters can be significantly different in upper-scale applications. Therefore, pilot-scale studies using environmentally relevant concentrations of model pollutants and large quantities of wastewater (>50 L) are required to assess the performance and sustainability of these approaches under semi-realistic conditions. For this reason, in the present study, pilot-scale experiments were carried out using the two processes that exhibited the highest FZ removal efficiency during lab-scale experiments, when SWW was used as a matrix (i.e., PS photoactivation and g-C_3N_4/PS hybrid approach). According to the results presented in Figure 1c, the removal of FZ during both applied processes was significantly slower (>40%) than that in the lab-scale experiments. The g-C_3N_4/PS method resulted in faster removal kinetics (~42%) than PS photoactivation, successfully removing approximately 86.7% of the initial concentration of FZ during the 120 min irradiation process. Overall, it could be suggested that the g-C_3N_4/PS hybrid process shows promise for effectively degrading persistent pollutants in aqueous matrices like SWW, potentially achieving a higher removal efficiency than heterogeneous photocatalysis with g-C_3N_4 or PS photoactivation under reasonable application time.

Photocatalyst recovery and reuse are critical factors that, in many cases, determine the viability of photocatalytic methods in upper-scale applications. In general, g-C_3N_4 is a well-established material whose properties have been extensively investigated in the last decade and, according to the results of relevant studies, retains its photocatalytic efficiency for at least three cycles when used in suspension form under lab-scale conditions for the remediation of aqueous media [78,79]. Interestingly, the reusability of g-C_3N_4 also appears to be unaffected when used in the presence of oxidants, as findings from studies investigating similar hybrid methodologies under lab-scale conditions indicate that it could be successfully reused for four cycles without significant loss of activity [80,81].

Therefore, it could be concluded that the hybrid approach proposed in this work could be sustainable to an extent as the photocatalyst is expected to be reusable, minimizing the operational costs.

Regarding the recovery of g-C_3N_4, various techniques have been proposed in the existing literature that could be utilized in recirculation systems such as the one used in the present study. In particular, the formation of g-C_3N_4 granules [82], the combination of g-C_3N_4 with magnetic materials [83], or its immobilization over bead-like materials [84] are techniques that allow the dispersion of the photocatalyst in the aqueous media as well as easier recovery at the end of the process. Overall, it appears that the hybrid g-C_3N_4/PS system has potential for use in upper-scale applications. However, the factors discussed above should be investigated in pilot-scale experiments in future studies to provide more concise data on the sustainability of the method.

3.2. Detection and Tentative Identification of FZ's TPs

To gain deeper insight into the performance of g-C_3N_4/PS in FZ removal, the transformation products (TPs) formed during the process were analyzed using UHPLC-LTQ-Orbitrap MS. Seven TPs were detected, with detailed HRMS data provided in Table 2. The tentative structural identification of these compounds was based on their chromatographic behavior, accurate pseudomolecular ion mass, and MS^2 fragmentation pattern. Additionally, the confidence level for each identification was determined based on the opinion report by Schymanski et al. and is included in Table 2 [85]. The proposed transformation pathways for FZ, based on the evolutionary profiles of the TPs, are depicted in Figure 2.

Table 2. HRMS data for FZ and its tentatively identified TPs.

Compound	t_R (min)	Theoretical $[M + H]^+/[M + Na]^+$	Experimental $[M + H]^+/[M + Na]^+$	Molecular Formula $[M + H]^+/[M + Na]^+$	Δ (ppm)	RDB	Fragment Ions	Confidence Level
FZ	6.46	226.0456	226.0454	$C_8H_8N_3O_5$	−1.756	6.5	139.13 113.19	1
			248.0269	$C_8H_7N_3O_5Na$	−3.554	6.5		
TP103	0.84	103.0499	103.0498	$C_3H_7N_2O_2$	−3.532	1.5	85.16 103.06	2b
		125.0321	125.0319	$C_3H_6N_2O_2Na$	−2.149	1.5		
TP104	0.79	104.0340	104.0339	$C_3H_6NO_3$	−2.687	1.5	86.03 104.04	3
TP111	1.19	111.0550	111.0549	$C_5H_7N_2O$	−3.326	3.5	94.03 111.05	3
TP129	1.66	129.0657	129.0658	$C_5H_9N_2O_2$	−0.341	2.5	112.03 94.03	2b
TP196	6.49	196.0711	196.0724	$C_8H_{10}N_3O_3$	3.888	5.5	88.04 96.00	2b
TP197	6.16	197.0557	197.0556	$C_8H_9N_2O_4$	−0.270	5.5	139.21 169.25	3
TP242	5.76	242.0407	242.0406	$C_8H_8N_3O_6$	−0.502	6.5	241.94 109.23	3
		264.0226	264.0225	$C_8H_7N_3O_6Na$	−0.705	6.5		

Note(s): Retention time (t_R), pseudo-molecular ion ($[M + H]^+$), mass error (Δ), ring and double bond equivalents (RDB).

TP103 appears to be formed directly via the photoinduced cleavage of the C=N bond of FZ (pathway 1) and is a common metabolite of the antibiotic known as AOZ (3-Amino-2-oxazolidinone) [48,86]. Furthermore, TP103 could potentially be produced (to a lesser extent) through the same mechanism by TP196 (pathway 3), and TP197 (pathway 4), as all these products contain this moiety in their respective proposed structures. The exact mass of the pseudo-molecular ion of TP242 differed from that of FZ by 15.9948 Da indicating that hydroxylation (-OH) of the parent compound occurred. However, the MS^2 data did not allow for the elucidation of the exact hydroxylation site; therefore, it is suggested that the most likely site is the one depicted in Figure 2c since 4-hydroxyfurazolidone is a well-known stable compound (pathway 2). TP196, which was detected at a relatively low concentration, was tentatively identified as the product generated through the reduction of FZ's nitro group (-NO_2) to an amino group (-NH_2) (pathway 3), which was probably mediated by the photogenerated electrons [49]. Similarly, TP197 (pathway 4) was identified as the product of the substitution of -NO_2 by -OH as the difference between the exact masses of FZ and TP197 was 28.9898 Da. The formation of TP111 (pathway 3) could be attributed to the cleavage of the N-N bond of TP197 as suggested in a recent study that focused on the photocatalytic removal of FZ [49]. In the case of TP129, the exact hydroxylation site could not be verified using the HRMS data. However, its evolutionary profile followed that of TP242 (Figure 2b), indicating a possible parent–product connection between the two. Therefore, the same hydroxylation site as in TP242 in the furan moiety was proposed. Based on this evidence, it appears that TP129 was formed through the cleavage of the N-N bond of TP242, followed by the reduction of the -NO_2 group and the C=N bond (pathway 2). Additionally, the formation of TP129 (to a lesser extent) via the cleavage of the N-N bond in TP196 followed by the hydroxylation of the furan moiety and reduction of the C=N bond could not be ruled out (Pathway 3). Finally, TP104 was tentatively identified as a linear molecule that could possibly be the derivative of TP103 after undergoing various reactions such as deamination and ring opening. This product was also identified in a relative study that applied a sonocatalytic approach using PS as an oxidant to degrade FZ [48].

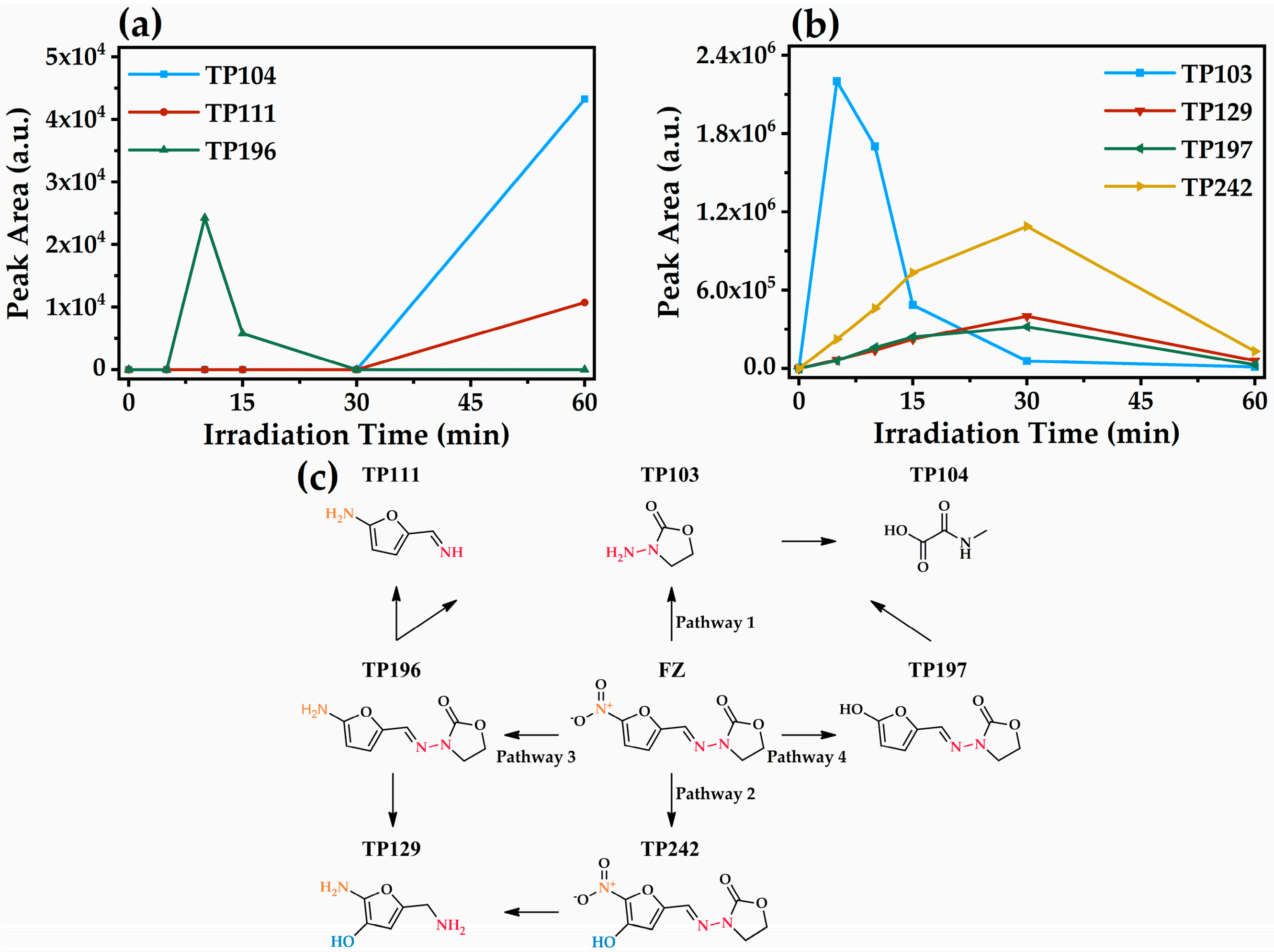

Figure 2. Evolutionary profiles of the tentatively identified (**a**) TP104, TP111, and TP196; (**b**) TP103, TP129, TP197, and TP242 of FZ generated under lab-scale conditions when the hybrid g-C_3N_4 approach was applied; and (**c**) the proposed transformation pathways of FZ.

3.3. Toxicity Assessment of the Photocatalytic Degradation of FZ with g-C_3N_4/PS

In general, AOPs are effective in removing harmful organic compounds from aqueous matrices, although in some cases, these techniques can lead to the formation of more toxic TPs than the parent compound, potentially increasing effluent toxicity [59]. Therefore, the determination of certain ecotoxicological parameters is necessary to assess whether the applied process has a positive effect in terms of environmental risk or whether it should be applied for longer time periods to achieve this.

3.3.1. In Vitro Ecotoxicological Assessment

The Microtox bioassay was employed to monitor the variations in the ecotoxicity of the reactor contents throughout the application of the hybrid photocatalytic process using g-C_3N_4/PS under both lab- and pilot-scale conditions. The lab-scale results (C_0 = 10 mg L^{-1}) presented in Figure 3a show that during the first 5 min, there was a sudden increase in ecotoxicity, which gradually decreased over the next 25 min. This observation could be related to the generation of more toxic TPs than the parent compound, as well as potential synergistic effects among them. After 45 min of irradiation, the initial bioluminescence inhibition was halved, indicating that the hybrid method achieved significant detoxification of the reactor content within this timeframe. However, at the end of the irradiation process, bioluminescence inhibition was 22% lower than the initial value (t = 0), suggesting that a higher degree of detoxification could potentially be achieved with a longer irradiation period.

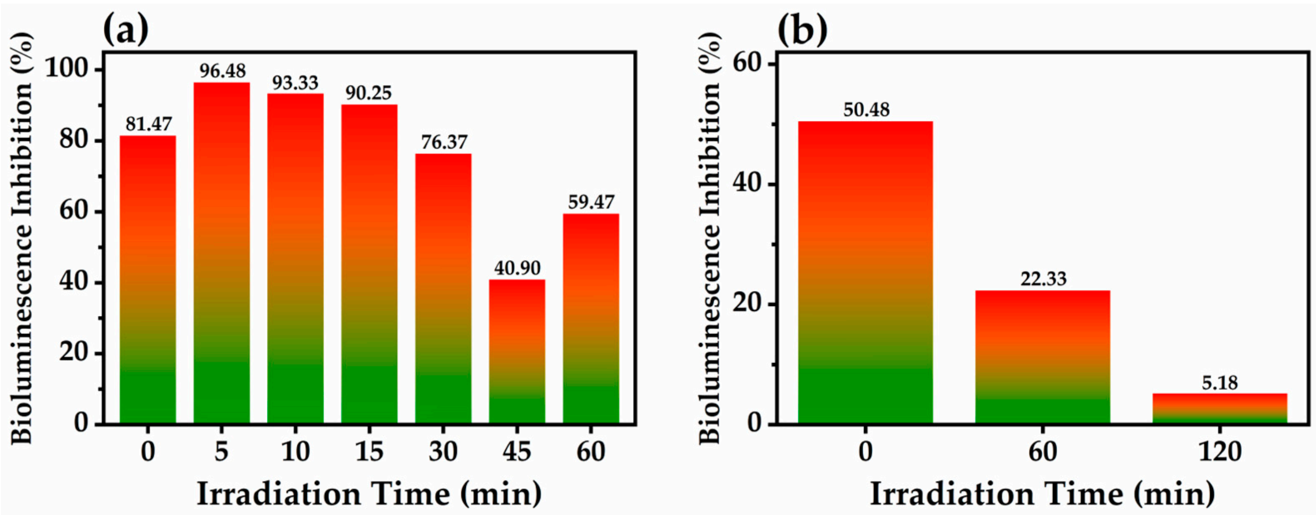

Figure 3. Bioluminescence inhibition of *V. fischeri* vs. irradiation time when g-C_3N_4/PS was utilized under (**a**) lab- and (**b**) pilot-scale conditions.

In the pilot-scale experiments, the spiked (C_0 = 250 μg L^{-1}) SWW matrix exhibited elevated toxicity, as the bioluminescence inhibition of *V. fischeri* was 50.48% before illumination (Figure 3b). After one hour of treatment with UV_A radiation in the presence of g-C_3N_4 and PS, the spiked SWW exhibited a significant reduction in toxicity (28.15%). Within 120 min of illumination, the initial bioluminescence inhibition was reduced by nearly tenfold, suggesting that the application of photocatalysis with g-C_3N_4 in the presence of PS is a viable, green approach to detoxify FZ-contaminated wastewater within a reasonable application time.

3.3.2. In Silico Ecotoxicological Risk Assessment for FZ and Its TPs

ECOSAR v2.0 was used to estimate the ecotoxicity values of FZ and its tentatively identified TPs for three trophic levels. To align these predictions with the Microtox bioassay results, LC_{50} values for daphnids were primarily considered, as *V. fischeri* shares greater biological similarity with aquatic crustaceans than with fish or green algae [59,87]. The software classifies compounds based on their structural features, usually into more than one chemical class (e.g., phenols). To facilitate the comparison of the predicted values, the category "hydrazines" was chosen as FZ and most of its TPs were included in this category.

According to the predicted in silico values presented in Table 3, all TPs, except TP111, were expected to be less toxic than FZ. These findings may explain the slight increase in bioluminescence inhibition in lab-scale experiments from 45 to 60 min of irradiation, as the formation of TP111 peaked within this time period (Figure 2a). However, they offered no obvious explanation for the sudden increase in ecotoxicity within the first 15 min, as none of the compounds generated during this timeframe were estimated to exhibit higher toxicity than the parent compound. This outcome could be explained by possible interactive effects among the TPs or the presence of TPs that were not detected by UHPLC-LTQ-Orbitrap MS analysis.

Table 3. In silico predicted LC_{50}/EC_{50}/ChV values of FZ and its TPs for fish daphnids and green algae. Chemical categories in the Compound column include: HZ: Hydrazines, AA: Aliphatic Amines, AN: Anilines, NO: Neutral Organics. Color code: red (Very Toxic), yellow (Toxic), blue (Harmful) to green (Non-Harmful).

Compound	Acute Toxicity			Chronic Toxicity		
	Fish LC_{50} (mg L^{-1})	Daphnid LC_{50} (mg L^{-1})	Green Algae EC_{50} (mg L^{-1})	Fish ChV (mg L^{-1})	Daphnid ChV (mg L^{-1})	Green Algae ChV (mg L^{-1})
FZ (HZ)	1.85	3.23	1.24	3.36	0.822	0.142
TP103 (HZ)	5.67	4.74	1.67	19.8	2.84	0.160
TP196 (HZ)	3.24	4.31	1.61	7.49	1.51	0.172
TP129 (AA)	1110	99.1	146	159	6.12	39.3
TP197 (HZ)	2.14	3.35	1.27	4.29	0.97	0.141
TP242 (HZ)	3.14	4.59	1.73	6.67	1.44	0.189
TP111 (AN)	71.5	2.31	7.42	1.17	0.025	3.31
TP104 (NO)	288,000	114,000	18,900	18,400	4040	2200

The predicted in silico mutagenicity and developmental toxicity values are summarized in Table 4. Notably, for TP129, no data were generated by this software. As can be observed, all TPs except TP242 exhibited lower mutagenicity values than FZ. Interestingly, the TPs formed at the end of the proposed pathways, namely TP103, TP104, and TP111, were labeled "Mutagenicity Negative" by TEST v5.1.2 as their predicted values were lower than 0.50. These findings indicate that the applied hybrid process has the potential to address a major problem associated with the mutagenic properties of FZ [88,89].

Table 4. In silico predicted mutagenicity and developmental toxicity values for FZ and its tentatively identified TPs.

Compound	Mutagenicity	Developmental Toxicity
FZ	1.01	0.64
TP103	0.44	0.81
TP104	0.11	0.65
TP111	0.40	0.69
TP129	N/A	N/A
TP196	0.91	0.69
TP197	0.91	0.80
TP242	1.01	0.67

In terms of developmental toxicity, the results were not as encouraging as those of mutagenicity. Specifically, all TPs demonstrated a higher affinity to induce toxic effects on embryos and developing organisms (Table 4), as their predicted developmental toxicity values were higher than that of FZ and were also labeled as "Developmental Toxicants".

Therefore, longer irradiation periods are suggested to degrade all identified TPs into less toxic molecules of low molecular weight, successfully limiting this specific problem.

4. Conclusions

The results of the present study highlight that the use of g-C_3N_4 in combination with PS is a prominent approach for the removal of recalcitrant toxic compounds from wastewater matrices compared to "stand-alone" techniques (e.g., photocatalysis with g-C_3N_4). Furthermore, the scalability of the g-C_3N_4/PS methodology was investigated through pilot-scale experiments and the findings showed that significant FZ degradation could be achieved within a reasonable application time and under environmentally relevant conditions, suggesting that this technique might be a promising alternative for practical applications.

The elucidation of the TPs using UHPLC-LTQ-Orbitrap MS provided insight into the degradation pathways of FZ and its fate upon the application of g-C_3N_4/PS. In addition, ecotoxicity studies have shown that a noteworthy reduction in ecotoxicity can be achieved when this method is applied to SWW under pilot-scale conditions, indicating that the utilization of this approach as a ternary treatment step in WWTPs might result in less toxic effluents.

Overall, it appears that the g-C_3N_4/PS system offers an efficient, scalable, and environmentally friendly approach for the degradation of emerging pollutants such as FZ. Future studies could focus on optimizing operational parameters for enhanced performance, evaluating the long-term stability of the catalyst, and investigating broader applications (i.e., by monitoring the removal of more emerging contaminants), to address the challenges of wastewater treatment in diverse scenarios, finally promoting sustainable approaches for contaminants removal.

Supplementary Materials: The following supporting information can be downloaded at: https://www.mdpi.com/article/10.3390/w17040602/s1. Table S1: Physicochemical characteristics of SWW sample used in lab and pilot-scale experiments; Table S2: Gradient elution program for the separation of FZ and its TPs; Table S3: Parameters of ESI-MS for the analysis of FZ and its TPs; Table S4: Removal kinetic constants (k), half-life values ($t_{1/2}$), percent removals of FZ, and correlation coefficients (R^2) per applied process; Table S5: Removal kinetic constants (k), half-life values ($t_{1/2}$), percent removals of FZ, and correlation coefficients (R^2) for different concentrations of PS in UWW (lab-scale); Table S6. Removal kinetic constants (k), half-life values ($t_{1/2}$), percent removals of FZ, and correlation coefficients (R^2) for different inorganic ions in UWW (lab-scale).

Author Contributions: Conceptualization, I.K., V.B. and T.A.; methodology, C.E., C.L. and V.B.; validation, C.E. and V.B.; formal analysis, C.E. and C.L.; investigation, C.E., C.L. and V.B.; resources, I.K. and T.A.; data curation, C.E. and C.L.; writing—original draft preparation, C.E. and C.L.; writing—review and editing, I.K. and V.B.; visualization, C.E. and C.L.; supervision, I.K. and T.A.; funding acquisition, I.K. and T.A. All authors have read and agreed to the published version of the manuscript.

Funding: The authors would like to thank the project "Advanced Nanostructured Materials for Sustainable Growth: Green Energy Production/Storage, Energy Saving and Environmental Remediation" (TAEDR-0535821), which is implemented under the action "Flagship actions in interdisciplinary scientific fields with a special focus on the productive fabric" (ID 16618), Greece 2.0—National Recovery and Resilience Fund, and funded by European Union NextGenerationEU.

Data Availability Statement: The original contributions presented in this study are included in the article/Supplementary Materials. Further inquiries can be directed to the corresponding author(s).

Acknowledgments: The authors would like to thank the Unit of Environmental, Organic and Biochemical high-resolution analysis–Orbitrap-LC–MS of the University of Ioannina for providing access to the facilities.

Conflicts of Interest: The authors declare no conflicts of interest.

References

1. Bidoglio, G.A.; Schwarzmueller, F.; Kastner, T. A Global Multi-Indicator Assessment of the Environmental Impact of Livestock Products. *Glob. Environ. Change* **2024**, *87*, 102853. [CrossRef]
2. Gržinić, G.; Piotrowicz-Cieślak, A.; Klimkowicz-Pawlas, A.; Górny, R.L.; Ławniczek-Wałczyk, A.; Piechowicz, L.; Olkowska, E.; Potrykus, M.; Tankiewicz, M.; Krupka, M.; et al. Intensive Poultry Farming: A Review of the Impact on the Environment and Human Health. *Sci. Total Environ.* **2023**, *858*, 160014. [CrossRef] [PubMed]
3. Kondor, A.C.; Molnár, É.; Jakab, G.; Vancsik, A.; Filep, T.; Szeberényi, J.; Szabó, L.; Maász, G.; Pirger, Z.; Weiperth, A.; et al. Pharmaceuticals in Water and Sediment of Small Streams under the Pressure of Urbanization: Concentrations, Interactions, and Risks. *Sci. Total Environ.* **2022**, *808*, 152160. [CrossRef]
4. Poikane, S.; Salas Herrero, F.; Kelly, M.G.; Borja, A.; Birk, S.; van de Bund, W. European Aquatic Ecological Assessment Methods: A Critical Review of Their Sensitivity to Key Pressures. *Sci. Total Environ.* **2020**, *740*, 140075. [CrossRef] [PubMed]
5. Darwish, W.S.; Thompson, L.A. Chapter 2—Soil, Water, and Air: Potential Contributions of Inorganic and Organic Chemicals. In *Present Knowledge in Food Safety*; Knowles, M.E., Anelich, L.E., Boobis, A.R., Popping, B., Eds.; Academic Press: Cambridge, MA, USA, 2023; pp. 26–43, ISBN 978-0-12-819470-6.
6. Morin-Crini, N.; Lichtfouse, E.; Liu, G.; Balaram, V.; Ribeiro, A.R.L.; Lu, Z.; Stock, F.; Carmona, E.; Teixeira, M.R.; Picos-Corrales, L.A.; et al. Emerging Contaminants: Analysis, Aquatic Compartments and Water Pollution. In *Emerging Contaminants Volume 1: Occurrence and Impact*; Morin-Crini, N., Lichtfouse, E., Crini, G., Eds.; Springer International Publishing: Cham, Switzerland, 2021; pp. 1–111, ISBN 978-3-030-69079-3.
7. Bavumiragira, J.P.; Ge, J.; Yin, H. Fate and Transport of Pharmaceuticals in Water Systems: A Processes Review. *Sci. Total Environ.* **2022**, *823*, 153635. [CrossRef] [PubMed]
8. Phoon, B.L.; Ong, C.C.; Mohamed Saheed, M.S.; Show, P.-L.; Chang, J.-S.; Ling, T.C.; Lam, S.S.; Juan, J.C. Conventional and Emerging Technologies for Removal of Antibiotics from Wastewater. *J. Hazard. Mater.* **2020**, *400*, 122961. [CrossRef]
9. Altowayti, W.A.H.; Shahir, S.; Othman, N.; Eisa, T.A.E.; Yafooz, W.M.S.; Al-Dhaqm, A.; Soon, C.Y.; Yahya, I.B.; Che Rahim, N.A.N.b.; Abaker, M.; et al. The Role of Conventional Methods and Artificial Intelligence in the Wastewater Treatment: A Comprehensive Review. *Processes* **2022**, *10*, 1832. [CrossRef]
10. dos Santos, D.F.; Moreira, W.M.; de Araújo, T.P.; Bergamasco, R.; Ostroski, I.C.; de Barros, M.A.S.D. Non-Conventional Processes Applied for the Removal of Pharmaceutics Compounds in Waters: A Review. *Process Saf. Environ. Prot.* **2022**, *167*, 527–542. [CrossRef]
11. Qamar, M.A.; Javed, M.; Shahid, S.; Shariq, M.; Fadhali, M.M.; Ali, S.K.; Khan, M.S. Synthesis and Applications of Graphitic Carbon Nitride (g-C_3N_4) Based Membranes for Wastewater Treatment: A Critical Review. *Heliyon* **2023**, *9*, e12685. [CrossRef] [PubMed]
12. Wang, H.; Li, X.; Zhao, X.; Li, C.; Song, X.; Zhang, P.; Huo, P.; Li, X. A Review on Heterogeneous Photocatalysis for Environmental Remediation: From Semiconductors to Modification Strategies. *Chin. J. Catal.* **2022**, *43*, 178–214. [CrossRef]
13. Antonopoulou, M.; Kosma, C.; Albanis, T.; Konstantinou, I. An Overview of Homogeneous and Heterogeneous Photocatalysis Applications for the Removal of Pharmaceutical Compounds from Real or Synthetic Hospital Wastewaters under Lab or Pilot Scale. *Sci. Total Environ.* **2021**, *765*, 144163. [CrossRef] [PubMed]
14. Sun, Y.; O'Connell, D.W. Application of Visible Light Active Photocatalysis for Water Contaminants: A Review. *Water Environ. Res.* **2022**, *94*, e10781. [CrossRef] [PubMed]
15. Ahmed, S.; Khan, F.S.A.; Mubarak, N.M.; Khalid, M.; Tan, Y.H.; Mazari, S.A.; Karri, R.R.; Abdullah, E.C. Emerging Pollutants and Their Removal Using Visible-Light Responsive Photocatalysis—A Comprehensive Review. *J. Environ. Chem. Eng.* **2021**, *9*, 106643. [CrossRef]
16. Marcelino, R.B.P.; Amorim, C.C. Towards Visible-Light Photocatalysis for Environmental Applications: Band-Gap Engineering versus Photons Absorption—A Review. *Environ. Sci. Pollut. Res.* **2019**, *26*, 4155–4170. [CrossRef] [PubMed]
17. Kumar, S.; Karthikeyan, S.; Lee, A.F. G-C_3N_4-Based Nanomaterials for Visible Light-Driven Photocatalysis. *Catalysts* **2018**, *8*, 74. [CrossRef]
18. Antonopoulou, M.; Tzamaria, A.; Miserli, K.; Lykos, C.; Konstantinou, I. Heterogeneous Photocatalytic Oxidation and Detoxification of Simulated Agricultural Wastewater Contaminated with Boscalid Fungicide Using G-C_3N_4 Catalyst. *Catalysts* **2024**, *14*, 112. [CrossRef]
19. Zhang, X.; Yuan, X.; Jiang, L.; Zhang, J.; Yu, H.; Wang, H.; Zeng, G. Powerful Combination of 2D G-C_3N_4 and 2D Nanomaterials for Photocatalysis: Recent Advances. *Chem. Eng. J.* **2020**, *390*, 124475. [CrossRef]
20. Wu, L.; Lu, Z.; Liao, J.; Xiang, X.; Song, H.; Yang, A.; Ibupoto, Z.H.; Lv, K. Photocatalytic Degradation of Sulfonamides in Suspensions of Coral-like Graphene Carbon Nitride with Nitrogen Vacancies. *Chemosphere* **2024**, *352*, 141313. [CrossRef] [PubMed]

21. Liu, D.; Li, C.; Zhao, C.; Zhao, Q.; Niu, T.; Pan, L.; Xu, P.; Zhang, F.; Wu, W.; Ni, T. Facile Synthesis of Three-Dimensional Hollow Porous Carbon Doped Polymeric Carbon Nitride with Highly Efficient Photocatalytic Performance. *Chem. Eng. J.* **2022**, *438*, 135623. [CrossRef]
22. Zhang, X.-W.; Lan, M.-Y.; Wang, F.; Yi, X.-H.; Wang, C.-C. ZIF-67-Based Catalysts in Persulfate Advanced Oxidation Processes (PS-AOPs) for Water Remediation. *J. Environ. Chem. Eng.* **2022**, *10*, 107997. [CrossRef]
23. Yang, J.; Zhu, M.; Dionysiou, D.D. What Is the Role of Light in Persulfate-Based Advanced Oxidation for Water Treatment? *Water Res.* **2021**, *189*, 116627. [CrossRef] [PubMed]
24. Wei, Z.; Villamena, F.A.; Weavers, L.K. Kinetics and Mechanism of Ultrasonic Activation of Persulfate: An in Situ EPR Spin Trapping Study. *Environ. Sci. Technol.* **2017**, *51*, 3410–3417. [CrossRef] [PubMed]
25. Xia, X.; Zhu, F.; Li, J.; Yang, H.; Wei, L.; Li, Q.; Jiang, J.; Zhang, G.; Zhao, Q. A Review Study on Sulfate-Radical-Based Advanced Oxidation Processes for Domestic/Industrial Wastewater Treatment: Degradation, Efficiency, and Mechanism. *Front. Chem.* **2020**, *8*, 592056. [CrossRef] [PubMed]
26. Liu, Z.; Ren, X.; Duan, X.; Sarmah, A.K.; Zhao, X. Remediation of Environmentally Persistent Organic Pollutants (POPs) by Persulfates Oxidation System (PS): A Review. *Sci. Total Environ.* **2023**, *863*, 160818. [CrossRef] [PubMed]
27. Lykos, C.; Tsalpatouros, K.; Fragkos, G.; Konstantinou, I. Synthesis, Characterization, and Application of Cu-Substituted $LaNiO_3$ Perovskites as Photocatalysts and/or Catalysts for Persulfate Activation towards Pollutant Removal. *Chemosphere* **2024**, *352*, 141477. [CrossRef]
28. Anipsitakis, G.P.; Dionysiou, D.D. Radical Generation by the Interaction of Transition Metals with Common Oxidants. *Environ. Sci. Technol.* **2004**, *38*, 3705–3712. [CrossRef]
29. Guerra-Rodríguez, S.; Rodríguez, E.; Singh, D.N.; Rodríguez-Chueca, J. Assessment of Sulfate Radical-Based Advanced Oxidation Processes for Water and Wastewater Treatment: A Review. *Water* **2018**, *10*, 1828. [CrossRef]
30. Wang, J.; Wang, S. Activation of Persulfate (PS) and Peroxymonosulfate (PMS) and Application for the Degradation of Emerging Contaminants. *Chem. Eng. J.* **2018**, *334*, 1502–1517. [CrossRef]
31. Hassani, A.; Scaria, J.; Ghanbari, F.; Nidheesh, P.V. Sulfate Radicals-Based Advanced Oxidation Processes for the Degradation of Pharmaceuticals and Personal Care Products: A Review on Relevant Activation Mechanisms, Performance, and Perspectives. *Environ. Res.* **2023**, *217*, 114789. [CrossRef]
32. Shiyi, Z.; Zhiruo, Z.; Dan, H.; Dongdong, Z.; Meizhen, W. Photoactivated Persulfate for Water and Wastewater Remediations: Mechanisms, Applications, and Catalysts. *Sep. Purif. Technol.* **2025**, *356*, 129829. [CrossRef]
33. Li, X.; Jie, B.; Lin, H.; Deng, Z.; Qian, J.; Yang, Y.; Zhang, X. Application of Sulfate Radicals-Based Advanced Oxidation Technology in Degradation of Trace Organic Contaminants (TrOCs): Recent Advances and Prospects. *J. Environ. Manag.* **2022**, *308*, 114664. [CrossRef] [PubMed]
34. Babaei, A.A.; Golshan, M.; Kakavandi, B. A Heterogeneous Photocatalytic Sulfate Radical-Based Oxidation Process for Efficient Degradation of 4-Chlorophenol Using TiO_2 Anchored on Fe Oxides@carbon. *Process Saf. Environ. Prot.* **2021**, *149*, 35–47. [CrossRef]
35. González-González, R.B.; Parra-Saldívar, R.; Alsanie, W.F.; Iqbal, H.M.N. Nanohybrid Catalysts with Porous Structures for Environmental Remediation through Photocatalytic Degradation of Emerging Pollutants. *Environ. Res.* **2022**, *214*, 113955. [CrossRef]
36. Gurav, R.; Bhatia, S.K.; Choi, T.-R.; Park, Y.-L.; Park, J.Y.; Han, Y.-H.; Vyavahare, G.; Jadhav, J.; Song, H.-S.; Yang, P.; et al. Treatment of Furazolidone Contaminated Water Using Banana Pseudostem Biochar Engineered with Facile Synthesized Magnetic Nanocomposites. *Bioresour. Technol.* **2020**, *297*, 122472. [CrossRef] [PubMed]
37. Saluti, G.; Ricci, M.; Castellani, F.; Rosato, R.; Colagrande, M.N.; Manucci, A.; Scortichini, G. Determination of Nitrofuran Metabolites in Muscle by LC-MS/MS and LC-MS/MS/MS: Alternative Validation According to Commission Implementing Regulation (EU) 2021/808. *Microchem. J.* **2024**, *199*, 110197. [CrossRef]
38. Fan, W.; Yang, S.; Gao, W.; Wang, D.; Fan, M. Highly Sensitive Bromide Aided SERS Detection of Furazolidone and 3-Amino-2-Oxazolidinone Residual in Aquaculture Products. *Microchem. J.* **2021**, *169*, 106532. [CrossRef]
39. Lewkowski, J.; Rogacz, D.; Rychter, P. Hazardous Ecotoxicological Impact of Two Commonly Used Nitrofuran-Derived Antibacterial Drugs: Furazolidone and Nitrofurantoin. *Chemosphere* **2019**, *222*, 381–390. [CrossRef] [PubMed]
40. Francesco, V.D.; Ierardi, E.; Hassan, C.; Zullo, A. Furazolidone Therapy for Helicobacter Pylori: Is It Effective and Safe? *World J. Gastroenterol.* **2009**, *15*, 1914. [CrossRef] [PubMed]
41. Graham, D.; Lu, H. Furazolidone in *Helicobacter Pylori* Therapy: Misunderstood and Often Unfairly Maligned Drug Told in a Story of French Bread. *Saudi J. Gastroenterol.* **2012**, *18*, 1–2. [CrossRef] [PubMed]
42. Le, V.V.H.; Olivera, C.; Spagnuolo, J.; Davies, I.G.; Rakonjac, J. In Vitro Synergy between Sodium Deoxycholate and Furazolidone against Enterobacteria. *BMC Microbiol.* **2020**, *20*, 5. [CrossRef] [PubMed]
43. Resina, E.; Gisbert, J.P. Rescue Therapy with Furazolidone in Patients with at Least Five Eradication Treatment Failures and Multi-Resistant H. Pylori Infection. *Antibiotics* **2021**, *10*, 1028. [CrossRef] [PubMed]

44. Zullo, A.; Ierardi, E.; Hassan, C.; De Francesco, V. Furazolidone-Based Therapies for Helicobacter Pylori Infection: A Pooled-Data Analysis. *Saudi J. Gastroenterol.* **2012**, *18*, 11. [CrossRef]
45. Wei, Y.-C.; Kumar Ghosh, M.; Yang, W.; Wang, J.; Wu, Z.-L.; Muddassir, M.; Kumar Ghorai, T. Synthesis and Characterization of Mixed Ligands Based Co(II)-Based Coordination Polymers and Study Their Photochemically Antibiotic Degradation. *Inorganica Chim. Acta* **2024**, *569*, 122133. [CrossRef]
46. Zhang, J.; Kumar Ghosh, M.; Yang, D.-C.; Muddassir, M.; Kumar Ghorai, T.; Jin, J.-C. A New 2,5-Bis(Pyrid-4-Yl)Pyridine Based Mn(II) Metal–Organic Framework on Photochemically Antibiotic Degradation. *Inorganica Chim. Acta* **2024**, *569*, 122132. [CrossRef]
47. Liu, X.; Ghosh, M.K.; Wang, J.; Zhong, X.; Muddassir, M.; Zhao, H.; Ghorai, K. Syntheses and Photochemically Antibiotic Degradation of Two Co(II)-Based Coordination Polymers. *Polyhedron* **2024**, *255*, 116958. [CrossRef]
48. Hadi Ghazvini, A.S.; Khataee, A.; Fathinia, M.; Haghighat, H.; Kudaibergenov, N. Sonocatalytic Degradation of Furazolidone Using a Heterogeneous Triple Ion Synergy System of ZnFe2O4@ZIF-67 Nanostructures: Physicochemical Characterization and Degradation Pathway. *Chem. Eng. J.* **2024**, *501*, 157273. [CrossRef]
49. Zhang, X.; Liu, R.; Liu, R.; Han, X.; Sun, Y.; Ren, B. Target Detection and Simultaneous Degradation of Furazolidone by Molecularly Imprinted CoWO4/g-C_3N_4. *Colloids Surf. Physicochem. Eng. Asp.* **2025**, *705*, 135694. [CrossRef]
50. Lykos, C.; Sioulas, S.; Konstantinou, I. G-C_3N_4 as Photocatalyst for the Removal of Metronidazole Antibiotic from Aqueous Matrices under Lab and Pilot Scale Conditions. *Catalysts* **2023**, *13*, 254. [CrossRef]
51. Durán, A.; Monteagudo, J.M.; Castillo, D.; Expósito, A.J. UV/Solar Photo-Degradation of Furaltadone in Homogeneous and Heterogeneous Phases: Intensification with Persulfate. *J. Environ. Manag.* **2022**, *319*, 115712. [CrossRef] [PubMed]
52. Hou, Y.; Yuan, G.; Wang, S.; Yu, Z.; Qin, S.; Tu, L.; Yan, Y.; Chen, X.; Zhu, H.; Tang, Y. Nitrofurazone Degradation in the Self-Biased Bio-Photoelectrochemical System: G-C_3N_4/CdS Photocathode Characterization, Degradation Performance, Mechanism and Pathways. *J. Hazard. Mater.* **2020**, *384*, 121438. [CrossRef]
53. Labriola, V.F.; Amaral, L.S.; Perussi, J.R.; Cavalheiro, C.C.S.; Azevedo, E.B. Nitrofurantoin Removal by the Photo-Fenton Process: Degradation, Mineralization, and Biological Inactivation. *Environ. Technol.* **2024**, *45*, 3418–3427. [CrossRef] [PubMed]
54. Szabó-Bárdos, E.; Cafuta, A.; Hegedűs, P.; Fónagy, O.; Kiss, G.; Babić, S.; Škorić, I.; Horváth, O. Photolytic and Photocatalytic Degradation of Nitrofurantoin and Its Photohydrolytic Products. *J. Photochem. Photobiol. Chem.* **2020**, *386*, 112093. [CrossRef]
55. Moles, S.; Mosteo, R.; Gómez, J.; Szpunar, J.; Gozzo, S.; Castillo, J.R.; Ormad, M.P. Towards the Removal of Antibiotics Detected in Wastewaters in the POCTEFA Territory: Occurrence and TiO_2 Photocatalytic Pilot-Scale Plant Performance. *Water* **2020**, *12*, 1453. [CrossRef]
56. Cabrera-Reina, A.; Martínez-Piernas, A.B.; Bertakis, Y.; Xekoukoulotakis, N.P.; Agüera, A.; Sánchez Pérez, J.A. TiO_2 Photocatalysis under Natural Solar Radiation for the Degradation of the Carbapenem Antibiotics Imipenem and Meropenem in Aqueous Solutions at Pilot Plant Scale. *Water Res.* **2019**, *166*, 115037. [CrossRef] [PubMed]
57. Fotiou, D.; Lykos, C.; Konstantinou, I. Photocatalytic Removal of the Antidepressant Fluoxetine from Aqueous Media Using TiO_2 P25 and G-C_3N_4 Catalysts. *J. Environ. Chem. Eng.* **2024**, *12*, 111677. [CrossRef]
58. Almansba, A.; Kane, A.; Nasrallah, N.; Wilson, J.M.; Maachi, R.; Lamaa, L.; Peruchon, L.; Brochier, C.; Amrane, A.; Assadi, A.A. An Engineering Approach towards the Design of an Innovative Compact Photo-Reactor for Antibiotic Removal in the Frame of Laboratory and Pilot-Plant Scale. *J. Photochem. Photobiol. Chem.* **2021**, *418*, 113445. [CrossRef]
59. Lykos, C.; Bairamis, F.; Efthymiou, C.; Konstantinou, I. Synthesis and Characterization of Composite WO_3 Fibers/g-C_3N_4 Photocatalysts for the Removal of the Insecticide Clothianidin in Aquatic Media. *Nanomaterials* **2024**, *14*, 1045. [CrossRef] [PubMed]
60. Efthymiou, C.; Boti, V.; Konstantinou, I.; Albanis, T. Aqueous Fate of Furaltadone: Kinetics, High-Resolution Mass Spectrometry—Based Elucidation and Toxicity Assessment of Photoproducts. *Sci. Total Environ.* **2024**, *919*, 170848. [CrossRef]
61. Song, L.; Zhu, B.; Jegatheesan, V.; Gray, S.; Duke, M.; Muthukumaran, S. Treatment of Secondary Effluent by Sequential Combination of Photocatalytic Oxidation with Ceramic Membrane Filtration. *Environ. Sci. Pollut. Res.* **2018**, *25*, 5191–5202. [CrossRef]
62. Lado Ribeiro, A.R.; Moreira, N.F.F.; Li Puma, G.; Silva, A.M.T. Impact of Water Matrix on the Removal of Micropollutants by Advanced Oxidation Technologies. *Chem. Eng. J.* **2019**, *363*, 155–173. [CrossRef]
63. Yang, Y.; Pignatello, J.J. Participation of the Halogens in Photochemical Reactions in Natural and Treated Waters. *Molecules* **2017**, *22*, 1684. [CrossRef] [PubMed]
64. Bilotta, G.S.; Brazier, R.E. Understanding the Influence of Suspended Solids on Water Quality and Aquatic Biota. *Water Res.* **2008**, *42*, 2849–2861. [CrossRef]
65. Reche, I.; Pace, M.L.; Cole, J.J. Modeled Effects of Dissolved Organic Carbon and Solar Spectra on Photobleaching in Lake Ecosystems. *Ecosystems* **2000**, *3*, 419–432. [CrossRef]
66. Wang, J.; Dou, M.; Wang, X.; Gao, B.; Zhuang, T.; Ma, Z. Synergetic Mechanism of Defective G-C_3N_4 Activated Persulfate on Removal of Antibiotics and Resistant Bacteria: ROSs Transformation, Electron Transfer and Noncovalent Interaction. *Chemosphere* **2022**, *294*, 133741. [CrossRef]

67. Shen, M.; Zhang, X.; Zhao, S.; Cai, Y.; Wang, S. A Novel Photocatalytic System Coupling Metal-Free Carbon/g-C_3N_4 Catalyst with Persulfate for Highly Efficient Degradation of Organic Pollutants. *Chemosphere* **2023**, *314*, 137728. [CrossRef] [PubMed]
68. Song, Y.; Huang, L.; Zhang, X.; Zhang, H.; Wang, L.; Zhang, H.; Liu, Y. Synergistic Effect of Persulfate and G-C_3N_4 under Simulated Solar Light Irradiation: Implication for the Degradation of Sulfamethoxazole. *J. Hazard. Mater.* **2020**, *393*, 122379. [CrossRef]
69. Shen, M.; Zhang, X.; Zhao, S.; Wang, S. gCN-P: A Coupled g-C_3N_4/Persulfate System for Photocatalytic Degradation of Organic Pollutants under Simulated Sunlight. *Environ. Sci. Pollut. Res.* **2022**, *29*, 23280–23291. [CrossRef]
70. Sun, H.; Guo, F.; Pan, J.; Huang, W.; Wang, K.; Shi, W. One-Pot Thermal Polymerization Route to Prepare N-Deficient Modified g-C_3N_4 for the Degradation of Tetracycline by the Synergistic Effect of Photocatalysis and Persulfate-Based Advanced Oxidation Process. *Chem. Eng. J.* **2021**, *406*, 126844. [CrossRef]
71. Gadore, V.; Ranjan Mishra, S.; Ahmaruzzaman, M. SnS2 Modified Carbonate-Intercalated Ni-Zn-Fe Trimetallic LDH as a Novel Photocatalyst for Persulfate Activation: Influence of Operational Parameters, Co-Existing Ions and Organic Compounds. *Chem. Eng. J.* **2023**, *475*, 146157. [CrossRef]
72. Wacławek, S.; Lutze, H.V.; Grübel, K.; Padil, V.V.T.; Černík, M.; Dionysiou, D.D. Chemistry of Persulfates in Water and Wastewater Treatment: A Review. *Chem. Eng. J.* **2017**, *330*, 44–62. [CrossRef]
73. Wang, Y.; Lin, Y.; He, S.; Wu, S.; Yang, C. Singlet Oxygen: Properties, Generation, Detection, and Environmental Applications. *J. Hazard. Mater.* **2024**, *461*, 132538. [CrossRef] [PubMed]
74. Pelaez, M.; Falaras, P.; Likodimos, V.; O'Shea, K.; de la Cruz, A.A.; Dunlop, P.S.M.; Byrne, J.A.; Dionysiou, D.D. Use of Selected Scavengers for the Determination of NF-TiO_2 Reactive Oxygen Species during the Degradation of Microcystin-LR under Visible Light Irradiation. *J. Mol. Catal. Chem.* **2016**, *425*, 183–189. [CrossRef] [PubMed]
75. Tavakoli Joorabi, F.; Kamali, M.; Sheibani, S. Effect of Aqueous Inorganic Anions on the Photocatalytic Activity of CuO–Cu2O Nanocomposite on MB and MO Dyes Degradation. *Mater. Sci. Semicond. Process.* **2022**, *139*, 106335. [CrossRef]
76. Vione, D. A Model Assessment of the Occurrence and Reactivity of the Nitrating/Nitrosating Agent Nitrogen Dioxide ($\bullet NO_2$) in Sunlit Natural Waters. *Molecules* **2022**, *27*, 4855. [CrossRef] [PubMed]
77. Kwon, B.G.; Kwon, J.-H. Measurement of the Hydroxyl Radical Formation from H_2O_2, NO_3^-, and Fe(III) Using a Continuous Flow Injection Analysis. *J. Ind. Eng. Chem.* **2010**, *16*, 193–199. [CrossRef]
78. Zebiri, Z.; Debbache, N.; Sehili, T. Sheet-like g-C_3N_4 for Enhanced Photocatalytic Degradation of Naproxen. *J. Photochem. Photobiol. Chem.* **2024**, *446*, 115189. [CrossRef]
79. Ganesan, S.; Kokulnathan, T.; Sumathi, S.; Palaniappan, A. Efficient Photocatalytic Degradation of Textile Dye Pollutants Using Thermally Exfoliated Graphitic Carbon Nitride (TE–g–C_3N_4). *Sci. Rep.* **2024**, *14*, 2284. [CrossRef] [PubMed]
80. Li, R.; Wu, Z.; Yang, Y.; Sun, S.; Ma, R.; Ding, H. Photocatalytic Persulfate Activation by Silica Microsphere-Supported g-C_3N_4 for Efficient Carbamazepine Degradation. *Mater. Sci. Semicond. Process.* **2024**, *184*, 108792. [CrossRef]
81. Gupta, S.; Gandhi, J.; Kokate, S.; Raikar, L.G.; Kopuri, V.G.; Prakash, H. Augmented Photocatalytic Degradation of Acetaminophen Using Hydrothermally Treated G-C_3N_4 and Persulfate under LED Irradiation. *Heliyon* **2023**, *9*, e16450. [CrossRef]
82. Panneri, S.; Ganguly, P.; Mohan, M.; Nair, B.N.; Mohamed, A.A.P.; Warrier, K.G.; Hareesh, U.S. Photoregenerable, Bifunctional Granules of Carbon-Doped g-C_3N_4 as Adsorptive Photocatalyst for the Efficient Removal of Tetracycline Antibiotic. *ACS Sustain. Chem. Eng.* **2017**, *5*, 1610–1618. [CrossRef]
83. Verma, A.; Sharma, G.; Wang, T.; Kumar, A.; Dhiman, P.; García-Peñas, A. Graphitic Carbon Nitride (g-C_3N_4)-Based Magnetic Photocatalysts for Removal of Antibiotics. *Carbon Lett.* **2024**. [CrossRef]
84. Balakrishnan, A.; Chinthala, M. Comprehensive Review on Advanced Reusability of G-C_3N_4 Based Photocatalysts for the Removal of Organic Pollutants. *Chemosphere* **2022**, *297*, 134190. [CrossRef]
85. Schymanski, E.L.; Jeon, J.; Gulde, R.; Fenner, K.; Ruff, M.; Singer, H.P.; Hollender, J. Identifying Small Molecules via High Resolution Mass Spectrometry: Communicating Confidence. *Environ. Sci. Technol.* **2014**, *48*, 2097–2098. [CrossRef]
86. Edhlund, B.L.; Arnold, W.A.; McNeill, K. Aquatic Photochemistry of Nitrofuran Antibiotics. *Environ. Sci. Technol.* **2006**, *40*, 5422–5427. [CrossRef]
87. Lykos, C.; Kourkouta, T.; Konstantinou, I. Study on the Photocatalytic Degradation of Metronidazole Antibiotic in Aqueous Media with TiO_2 under Lab and Pilot Scale. *Sci. Total Environ.* **2023**, *870*, 161877. [CrossRef] [PubMed]
88. Zhou, Y.; Wang, J.; Wu, B.; Zhu, B. Rapid Determination of Furazolidone Residues in Animal Foods by Time-Resolved Fluorescence Immunochromatography. *Food Chem.* **2024**, *445*, 138711. [CrossRef]
89. Zhang, W.; Niu, Z.; Yin, K.; Liu, F.; Chen, L. Degradation of Furazolidone by Bacteria *Acinetobacter calcoaceticus* T32, *Pseudomonas putida* SP1 and *Proteus mirabilis* V7. *Int. Biodeterior. Biodegrad.* **2013**, *77*, 45–50. [CrossRef]